Yamane J, Nakamura M, Iwanami A, Sakaguchi M, Katoh H, Yamada M, Momoshima S, Miyao S, Ishii K, Tamaoki N, Nomura T, Okano HJ, Kanemura Y, Toyama Y, Okano H.	Transplantation of Galectin-1 -Expressing Human Neural Stem Cells into the Injured Spinal Cord of Adult Common Marmosets.	J Neurosci Res	88	1394-1405	2009
Shibata S, Yasuda A, Renault-Mihara F, Suyama S, Katoh H, Inoue T, Inoue YU, Nagoshi N, Sato M, Nakamura M, Akazawa C, Okano H.	Sox10-Venus mice: a new tool for real-time labeling of neural crest lineage cells and oligodendrocytes.	Mol Brain	3	31	2010
Mukaino M, Nakamura M, Yamada O, Okada S, Morikawa S, Renault-Mihara F, Iwanami A, Ikegami T, Ohsugi Y, Tsuji O, Katoh H, Matsuzaki Y, Toyama Y, Liu M, Okano H.	Anti-IL-6-receptor antibody promotes repair of spinal cord injury by inducing microglia-dominant inflammation	Exp Neurol	224	403-414	2010
Takahashi Y, Tsuji O, Kumagai G, Hara CM, Okano HJ, Miyawaki A, Toyama Y, Okano H, Nakamura M.	Comparative study of methods for administering neural stem/progenitor cells to treat spinal cord injury in mice.	Cell Transplant	20	727-739	2011
Tsuji O, Miura K, Okada Y, Fujiyoshi K, Mukaino M, Nagoshi N, Kitamura K, Kumagi G, Nishino M, Tomisato S, Higashi H, Nagai T, Katoh H, Kohda K, Matsuzaki Y, Yuzaki M, Ikeda E, Toyama Y, Nakamura M, Yamanaka S, Okano H.	Therapeutic potential of appropriately evaluated safe-induced pluripotent stem cells for spinal cord injury	PNAS	107	12704-12709	2010

Shinozaki M, Takahashi Y, Mukaino M, Saito N, Toyama Y, Okano H, Nakamura M.	Novel Concept of Motor Functional Analysis for Spinal Cord Injury in Adult Mice.	Journal of Biomedicine and Biotechnology		157458	2011
Shimo K, Ueno T, Younger J, Nishihara M, Inoue S, Ikemoto T, Taniguchi S, Ushida T.	Visualization of painful experiences believed to trigger the activation of affective and emotional brain regions in subjects with low back pain.	PLoS One	6	e26681	2011
Nagamoto Y, Ishii T, Sakaura H, Iwasaki M, Morimoto H, Kashii M, Hattori T, Yoshikawa H, Sugamoto K.	In vivo three-dimensional kinematics of the cervical spine during head rotation in patients with cervical spondylosis.	Spine	36	778-783	2011
Fujimori T, Iwasaki M, Okuda S, Nagamoto Y, Sakaura H, Oda T, Yoshikawa H.	Patient satisfaction with surgery for cervical myelopathy due to ossification of the posterior longitudinal ligament.	J Neurosurg Spine	14	726-733	2011
Hattori T, Sakaura H, Iwasaki M, Nagamoto Y, Yoshikawa H, Sugamoto K.	In vivo three-dimensional segmental analysis of adolescent idiopathic scoliosis.	Eur Spine J	20	1745-1750	2011
Fujimori T, Iwasaki M, Nagamoto Y, Ishii T, Sakaura H, Kashii M, Yoshikawa H, Sugamoto K.	Three-dimensional measurement of growth of ossification of the posterior longitudinal ligament.	J Neurosurg Spine	16	289-295	2012
Nakamura M, Fujiyoshi K, Tsuji O, Konomi T, Hosogane N, Watanabe K, Tsuji T, Ishii K, Momoshima S, Toyama Y, Chiba K, Matsumoto M.	Clinical significance of diffusion tensor tractography as a prognostic predictor of functional recovery in cervical compressive myelopathy patients after laminoplasty.	J Neurosurg	(in press)		2012

Okada S, Nakamra M, Saiwai H, Kumamaru H, Toyama Y, Iwamoto Y, Okano H.	Physiological signinficance of astrogliosis after CNS injury.	Inflammation and Regeneration	29	35-39	2009
Nagoshi N, Shibata S, Nakamura M, Matsuzaki Y, Toyama Y, Okano H.	Neural crest-derived stem cells display a wide variety ofcharacteristics.	Journal of Cellular Biochemistry	107	1046-1052	2009
Nakamura M, Nagoshi N, FujiyoshiK, Kaneko S, Toyama Y, Okano H.	Regenerative medicine for spinal cord injury-Current Status and Open Issues-	Inflammation and Regeneration	29	198-203	2009
Miura K, Tsuji O, Nakamura M, Okano H.	Toward using iPS cells to treat spinal cord injury: Their safety and therapeutic efficacy.	Inflammation and Regeneration	31	2-10	2011
Funao H, Ishii K, Nagai S, Sasaki A, Hoshikawa T, Aizawa M, Okada Y, Chiba K, Koyasu S, Toyama Y, Matsumoto M.	Establishment of a Real-Time,Quantitative,and Reproducible Mouse Model of Staphylococcus Osteomyelitis Using Bioluminescence Imagin	Infect Immun	80	733-741	2012
辻収彦, 岡野栄之	脊髄損傷へのES/iPS細胞由来神経幹細胞移植	実験医学	28	223-229	2010
金子慎二郎, 中村雅也,戸山芳昭, 岡野栄之	脊髄損傷後の軸索再生制御機構の解明と軸索再生促進へのストラテジー	慶應医学	85	191-195	2009
藤吉兼浩, 辻収彦, 松本守雄,千葉一裕, 戸山芳昭, 中村雅也	脊髄領域における画像診断技術の最近の進歩　拡散テンソルtractography	脊椎脊髄ジャーナル	23	315-323	2010

岡野栄之，辻収彦，三浦恭子,岡田洋平，藤吉兼浩,高木岳彦，金子慎二郎，戸山芳昭,山中伸弥，中村雅也	中枢神経系と末梢神経系の再生戦略	Peripheral Nerve 末梢神経	21	145-151	2010
辻収彦，名越慈人，藤吉兼浩，戸山芳昭，岡野栄之，中村雅也	脊髄損傷に対するiPS細胞および神経堤幹細胞移植	脊椎脊髄	23	818-827	2010
三浦恭子，辻収彦，岡野栄之	iPS細胞の安全性の担保.	再生医療	9	315-322	2010
辻収彦，中村雅也，岡野栄之	iPS細胞を利用した神経再生	細胞	42	504-508	2010
熊谷玄太郎，岡田洋平，藤哲，戸山芳昭，中村雅也，岡野栄之	脊髄損傷に対するＥＳ細胞由来神経幹細胞一移植	脊椎脊髄ジャーナル	23	835-844	2010
安田明正，辻収彦，藤吉兼浩，戸山芳昭，岡野栄之，中村雅也	【脊髄損傷治療の現状とこれから】 人工多能性幹(iPS)細胞を用いた脊髄損傷治療	脳21	14	126-132	2011
向野雅彦,中村雅也	損傷脊髄の再生医療	Journal of Clinical Rehabilitation	20	456-459	2011
辻収彦，戸山芳昭，中村雅也	【脊髄損傷-その研究成果と臨床の現状】脊髄損傷の基礎研究　細胞関連iPS細胞由来神経幹細胞.	Bone Joint Nerve	1	439-445	2011
辻収彦，三浦恭子，中村雅也，岡野栄之	【iPS 細胞の再生医療の実現へ向けた動向】 iPS 細胞の安全性と脊髄損傷への応用	細胞	43	371-375	2011
小林喜臣，海苔聡，安田明正，岡田洋平，藤吉兼浩，辻収彦，戸山芳昭，中村雅也，岡野栄之	【iPS細胞の臨床応用の展望】 iPS細胞を用いた脊髄再生医療の最前線.	BIO Clinica	26	781-786	2011

海苔聡, 辻収彦, 戸山芳昭, 岡野栄之, 中村雅也	iPS細胞由来神経幹細胞移植による脊髄損傷治療.	整災外	54	1132-1133	2011
高橋勇一朗, 岡野栄之, 戸山芳昭, 中村雅也	整形外科領域における蛍光イメージング　脊髄再生関連　神経幹細胞の蛍光発光標識によるイメージングと応用	臨整外	47	7-15	2012
船尾陽生, 石井賢, 蔵本哲也, 塩野雄太, 吉岡研之, 石濱寛子, 中村雅也, 戸山芳昭, 千葉一裕, 松本守雄	誌上シンポジウム　整形外科領域における蛍光イメージング　整形外科の基礎研究における蛍光・バイオイメージング法　感染症領域への応用	臨整外	47	43-49	2012

Ⅲ. 研究成果の刊行物・別刷

NeuroImage 44 (2009) 884–892

Contents lists available at ScienceDirect

NeuroImage

journal homepage: www.elsevier.com/locate/ynimg

Visualization of peripheral nerve degeneration and regeneration: Monitoring with diffusion tensor tractography☆

Takehiko Takagi [a,b], Masaya Nakamura [a], Masayuki Yamada [e,f], Keigo Hikishima [d,e], Suketaka Momoshima [c], Kanehiro Fujiyoshi [a,b], Shinsuke Shibata [b], Hirotaka James Okano [b], Yoshiaki Toyama [a], Hideyuki Okano [b,*]

[a] Department of Orthopaedic Surgery, Keio University School of Medicine, 35 Shinanomachi, Shinjuku-ku, Tokyo 160-8582, Japan
[b] Department of Physiology, Keio University School of Medicine, 35 Shinanomachi, Shinjuku-ku, Tokyo 160-8582, Japan
[c] Department of Diagnostic Radiology, Keio University School of Medicine, 35 Shinanomachi, Shinjuku-ku, Tokyo 160-8582, Japan
[d] Center for Integrated Medical Research, Keio University, 35 Shinanomachi, Shinjuku-ku, Tokyo 160-8582, Japan
[e] Central Institute for Experimental Animals, 1430 Nogawa, Miyamae-ku, Kawasaki, Kanagawa, 216-0001, Japan
[f] Faculty of Radiological Technology, Fujita Health University School of Health Sciences, 1-98 Dengakugakubo, Kutsukake-cho, Toyoake-shi, Aichi 470-1192, Japan

ARTICLE INFO

Article history:
Received 1 July 2008
Revised 15 September 2008
Accepted 17 September 2008
Available online 2 October 2008

Keywords:
Diffusion tensor imaging
Diffusion tensor tractography
Peripheral nerve injury
Fractional anisotropy
Wallerian degeneration
Magnetic resonance imaging

ABSTRACT

We applied diffusion tensor tractography (DTT), a recently developed MRI technique that reveals the microstructures of tissues based on its ability to monitor the random movements of water molecules, to the visualization of peripheral nerves after injury. The rat sciatic nerve was subjected to contusive injury, and the data obtained from diffusion tensor imaging (DTI) were used to determine the tracks of nerve fibers (DTT). The DTT images obtained using the fractional anisotropy (FA) threshold value of 0.4 clearly revealed the recovery process of the contused nerves. Immediately after the injury, fiber tracking from the designated proximal site could not be continued beyond the lesion epicenter, but the intensity improved thereafter, returning to its pre-injury level by 3 weeks later. We compared the FA value, a parameter computed from the DTT data, with the results of histological and functional examinations of the injured nerves, during recovery. The FA values of the peripheral nerves were more strongly correlated with axon-related (axon density and diameter) than with myelin-related (myelin density and thickness) parameters, supporting the theories that axonal membranes play a major role in anisotropic water diffusion and that myelination can modulate the degree of anisotropy. Moreover, restoration of the FA value at the lesion epicenter was strongly correlated with parameters of motor and sensory functional recovery. These correlations of the FA values with both the histological and functional changes demonstrate the potential usefulness of DTT for evaluating clinical events associated with Wallerian degeneration and the regeneration of peripheral nerves.

Introduction

MRI, an indispensable tool in the diagnosis of central nervous system disorders, has rarely been applied to diseases of the peripheral nervous system, because it is difficult to delineate peripheral nerves on account of their poor contrast with the surrounding tissues. The standard repertoire for diagnosing peripheral nerve disorders includes clinical and electrophysiological examinations, supplemented by more invasive procedures.

For the differential diagnosis of peripheral nerve lesions, the visualization of peripheral nerves using MRI has been attempted using special techniques such as MR neurography (Filler et al., 2004; Howe et al., 1992). However, the interpretation of the images obtained by MR neurography is based on visual inspection, and is therefore qualitative and subjective. Furthermore, since MR neurography cannot image continuous nerve fibers over their entire length, it is not considered useful for examining the growth of regenerating peripheral nerves. To visualize nerve fibers in MRI, a contrast agent such as superparamagnetic iron oxide (SPIO) (Bendszus and Stoll, 2003) or gadofluorine M (Bendszus et al., 2005; Wessig et al., 2008) can be injected, but this is invasive. The difficulty in visualizing axons makes these methods impractical for evaluating peripheral nerve injury in the present clinical scenario.

To overcome these shortcomings, here we applied diffusion tensor imaging (DTI), a non-invasive method that reveals the microstructure of tissues on the basis of its ability to monitor the random movements of water molecules (Basser et al., 1994). Diffusion tensor tractography (DTT) refers to the analysis and reconstruction of the data obtained by DTI, by which the orientation of nerve fibers can be followed to trace specific neural pathways, such as that of the corticospinal tract in the brain or the spinal cord (Conturo et al., 1999; Fujiyoshi et al., 2007; Mori and Zhang, 2006; Tuch et al., 2001). Mac Donald et al have

☆ Diffusion tensor peripheral nerve tractography.

* Corresponding author. Fax: +81 3 3357 5445.
E-mail address: hidokano@sc.itc.keio.ac.jp (H. Okano).

1053-8119/$ – see front matter © 2008 Elsevier Inc. All rights reserved.
doi:10.1016/j.neuroimage.2008.09.022

obtained results indicating that DTI may be more sensitive than conventional MRI for evaluating traumatic brain injury (Mac Donald et al., 2007b).

Recent advances in MRI technology have made it possible to delineate peripheral nerve tracts in humans (Hiltunen et al., 2005; Meek et al., 2006; Skorpil et al., 2004). However, the reliability of DTT imaging has not yet been validated with detailed histological studies and quantitative analyses, so it has remained unclear whether the changes in DTT parameters actually correspond to the anatomical degeneration and regeneration of axonal fibers. Although the disintegration of axonal structures and demyelination occurring after peripheral nerve injury, known as Wallerian degeneration, is known to reduce the anisotropy of peripheral nerves (Beaulieu et al., 1996; Stanisz et al., 2001), and DTI has been shown to be useful for detecting axonal injury after traumatic brain injury (Mac Donald et al., 2007a,b) and ischemic injury of the optic nerve (Song et al., 2003; Sun et al., 2008), peripheral nerve tracking during the process of Wallerian degeneration has never been reported. We believe that since no proper tools are presently available for the visualization of peripheral nerves, it is important to evaluate the validity of applying DTT to assess peripheral nerve degeneration and regeneration. The objectives of the present study were to determine whether DTT is useful for tracking peripheral nerves, and to determine the relevance of the tracking parameters for evaluating fibers after peripheral nerve injury, by comparing them with histological and functional parameters of recovery.

Materials and methods

Animals and surgical procedures

One hundred twenty adult female Sprague-Dawley rats (165–228 g, 7 or 8 weeks of age; Clea Japan Inc., Tokyo, Japan) were used. All interventions and animal care procedures were performed in accordance with the Laboratory Animal Welfare Act, the Guide for the Care and Use of Laboratory Animals (National Institutes of Health), and the Guidelines and Policies for Animal Surgery provided by the Animal Study Committee of Keio University, and were approved by the Ethics Committee of Keio University. All surgeries were performed under chloral hydrate anesthesia (intraperitoneal injection; 350 mg per kg body weight; Wako Pure Chemicals, Osaka, Japan). The animals were housed in groups under a 12-hour light/dark cycle, with access to food and water *ad libitum*. The sciatic nerve was exposed through a dorsal gluteal muscle-splitting approach. The nerve was then subjected to a contusive injury at the sciatic notch using a brain aneurysm clip (Sugita clip; Mizuho Ikakogyo, Tokyo, Japan). The clip was closed and left in place for 5 min with a holding force of approximately 150 g (Kato et al., 2005).

Magnetic resonance imaging

MRI was performed using a 7.0-Tesla magnet (PharmaScan 70/16; Bruker BioSpin, Ettlingen, Germany) with a 38-mm volume coil dedicated for examinations of small animals. In studies using excised sciatic nerve, intact (pre-injured) excised nerves and nerves that had been excised 3 h, 1 day, 4 days, and 1, 2, 3, 4, 6, 8, and 12 weeks after the crush injury ($n=10$ each) were embedded in 2% agarose gel with 5 mM copper sulfate, and immediately subjected to diffusion tensor MRI. DTI data sets were acquired with a spin-echo sequence based on the Stejskal-Tanner diffusion preparation (Stejskal and Tanner, 1965). The scanning parameters were as follows: repetition time (TR), 15,000 ms; echo time (TE), 40 ms; flip angle, 90°; field of view (FOV), 40×40 mm; acquisition data matrix, 128×128; reconstructed image resolution, 0.31 mm; slice thickness, 0.94 mm; number of excitations (NEX), 1; b-value, 1000 s/mm^2; and motion probing gradient (MPG) orientations, 12 axes. Table 1 shows our normalized diffusion gradient orientations; duration of diffusion gradient pulses, 7 ms; diffusion time, 14 ms. The total imaging time was 6 h, 56 min.

Table 1
Normalized diffusion gradient orientations

Image volume	Gradients		
	x	*y*	*z*
1	0.0000	0.0000	0.0000
2	0.8944	0.0000	0.4472
3	0.0000	0.4472	0.8944
4	0.4472	0.8944	0.0000
5	0.8944	0.4472	0.0000
6	0.0000	0.8944	0.4472
7	0.4472	0.0000	0.8944
8	0.8944	0.0000	−0.4472
9	0.0000	−0.4472	0.8944
10	−0.4472	0.8944	0.0000
11	0.8944	−0.4472	0.0000
12	0.0000	0.8944	−0.4472
13	−0.4472	0.0000	0.8944

Diffusion tensor analysis

Diffusion tensor tractographic images were computed using the Volume One and dTV II SR software (Masutani et al., 2003). The diffusion tensor can be represented as an ellipsoid, where a proton at the center of the voxel has an equal probability of diffusing to any point in that ellipsoid. The eigenvectors of the diffusion tensor represent the three axes of the ellipsoid, namely, the length of the longest, middle, and shortest axes (called eigenvalues λ_1, λ_2 and λ_3). The eigenvector (e_1) associated with the largest eigenvalue (λ_1) was assumed to represent the local fiber direction. Fiber tracking was initiated from a manually selected region of interest (ROI), from which tracking lines were propagated bidirectionally according to the principal eigenvector (e_1) in each voxel. For the tractography, the ROI was placed at a site 5 mm proximal to the lesion epicenter, and the direction of the diffusion anisotropy was followed until the tracking was terminated at a voxel, depending on the threshold selected, with a fractional anisotropy (FA) of less than 0.25, 0.3, 0.4, 0.5, 0.6, 0.7, or 0.75. The FA value, a convenient index because it is scaled from 0 (isotropic) to 1 (anisotropic) (Mori and Zhang, 2006), can be calculated from the degree of diffusion anisotropy (Pierpaoli and Basser, 1996).

We determined the FA values and three eigenvalues (λ_1, λ_2, and λ_3) in each specimen at points 5 mm (proximal site), 0 mm (lesion epicenter), and −5 mm (distal site) from the lesion epicenter.

Histological analysis

Toluidine blue staining (light microscopy)

Samples were fixed in 2.5% glutaraldehyde/0.1 M cacodylate buffer (pH 7.4) for 12 h, then washed in cacodylate buffer, post-fixed for 2 h in 1% OsO_4/0.1 M cacodylate buffer (pH 7.4), dehydrated in a graded alcohol series and acetone, and finally embedded in epoxy resin. Semi-thin sections (1 μm thick) were cut cross-sectionally from the injured nerve specimens from a site 5 mm distal to the lesion epicenter and at the lesion epicenter at 4 days, 3 weeks, and 12 weeks after the crush injury, and stained with toluidine blue (1%) for 20 min; the corresponding sections from intact nerve specimens were also examined. The stained sections were then examined under a light microscope (AxioCam 2; Carl Zeiss, Jena, Germany).

Uranyl acetate staining (electron microscopy)

Ultrathin sections (80 nm thick) were obtained from the intact and injured nerve specimens at the same sites and time points as for the light microscopic examination, and stained with uranyl acetate (4.7%) for 30 min and Reynold's lead citrate for 8 min. Micrographs from 20 random fields of 17×17 μm^2 were obtained under a transmission

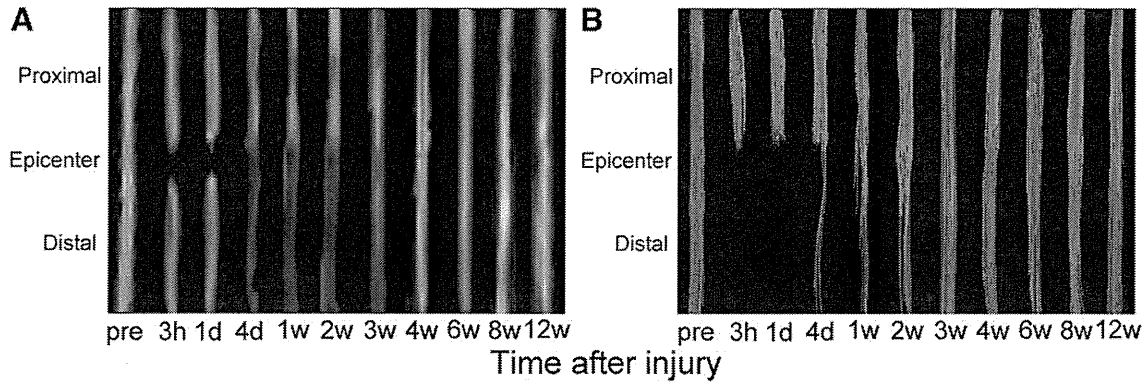

Fig. 1. FA map (A) and diffusion tensor tractography (B) of intact and injured sciatic nerves. For the tractography, the region of interest (ROI) was placed 5 mm proximal to the lesion epicenter. The FA value threshold was set at 0.4. In the DTT image constructed using this FA threshold value, the recovery process of the contused peripheral nerves could be clearly detected under the imaging parameters used.

electron microscope (JEOL model 1230; JEOL Ltd., Tokyo, Japan), by Digital Micrograph 3.3 (Gatan Inc., Warrendale, Pennsylvania, USA).

Quantitative analysis

Nerve samples were obtained at each of the ten time points used for diffusion tensor analysis, and subjected to quantitative determinations at the distal site, at which Wallerian degeneration/regeneration occurred. The following parameters were calculated for each nerve using the MCID system (Imaging Research, Inc., Toronto, Ontario, Canada): axon density, axon diameter, myelin sheath density, and myelin sheath thickness. Axon density was defined as axonal area/ total area, and myelin sheath density was defined as myelin sheath area/ total area in a fascicle in each nerve sample. The axon diameter and myelin sheath thickness of 40 randomly selected axons were

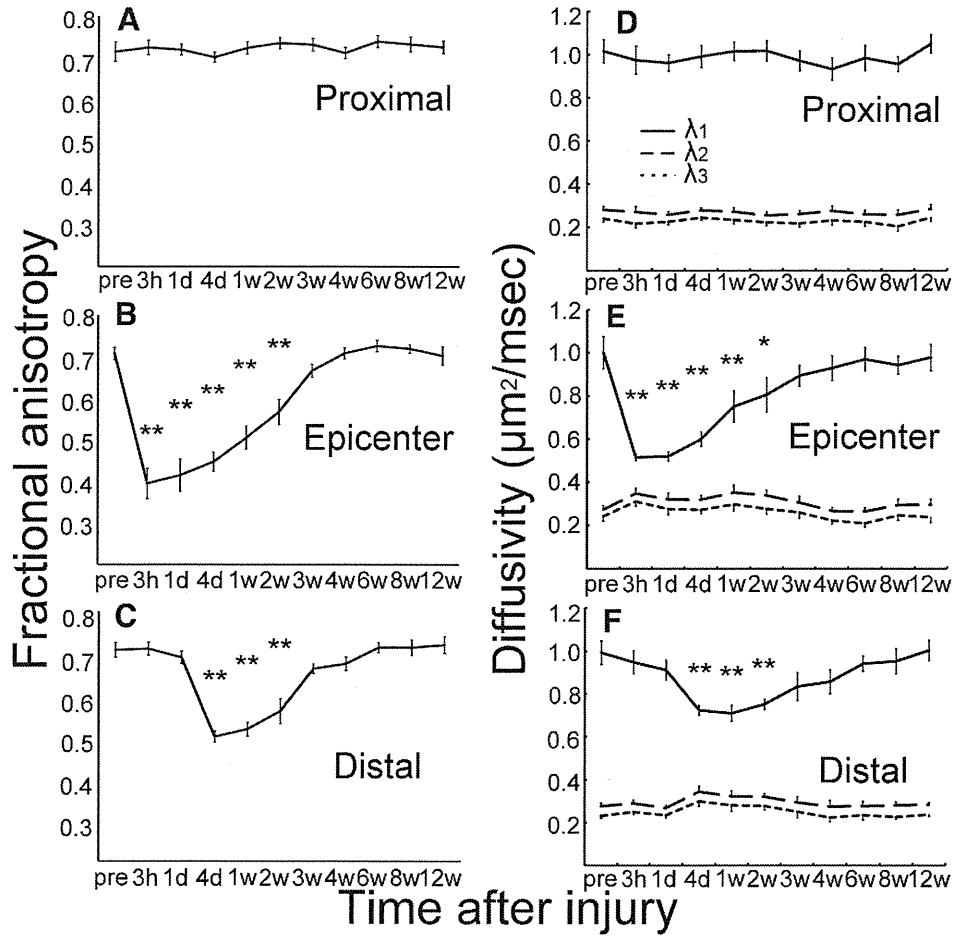

Fig. 2. Quantitative and temporal analysis of the FA values (A, proximal site; B, epicenter site; C, distal site), and eigenvalues (D, proximal site; E, epicenter site; F, distal site) ($n=10$ each). At the lesion epicenter, the FA value decreased sharply at 3 h and recovered gradually, reaching the pre-injury level by 3 weeks after the injury (B). At the distal site, while no significant change in the FA value was observed at 3 h or 1 day after the injury, a decrease was observed at 4 days, with gradual recovery thereafter to the pre-injury level by 3 weeks after the injury (C). The present model showed that both λ_2 and λ_3 were more constant than λ_1 (D–F), and that changes in FA values during the recovery after peripheral nerve injury depended mainly on λ_1, which represents the diffusivity along the longitudinal axis of the nerve. Statistical significance was determined to be $P<0.05$ using Dunnett's multiple comparison. Data represent the mean±SEM. *$P<0.05$; **$P<0.01$.

measured in each nerve sample. We also examined the changes in the distribution of the axon diameter after injury.

Behavioral analysis

Three different tests were used to assess the functional recovery after sciatic nerve injury. Ten rats were used for each functional evaluation. Each rat was examined at the same time-points used for the diffusion tensor analysis.

Leg muscle contraction test

The motor function of the lower extremities of the animals was evaluated using the leg muscle contraction test, in which isometric plantar flexion at the ankle is tested by pushing the sole until the toe touches the knee. A digital force gauge (Nidec-Shimpo Corp., Kyoto, Japan) was used for this test. The ratio of the degree of muscle contraction on the injured side to that on the contralateral sham-operated side was averaged.

Rota-rod test

The motor coordination of the animals was assessed using a rotating rod apparatus (Muromachi Kikai Co., Ltd., Tokyo, Japan) consisting of a plastic rod (9 cm in diameter) with a gritted surface, flanked by two large discs (50 cm in diameter) to prevent interference from other animals, at a height of 20 cm from the floor. The experimental rat was placed on the rod, and the rod was rotated at a speed of 15 rpm, following acclimation sessions (3 trials each at 5 and 10 rpm). The latency period until the rats fell off the apparatus was monitored for 180 s.

von Frey filament test

The mechanical sensitivity, which is the capacity of a sense organ to respond to mechanical stimulation, of the animals was tested using von Frey filaments (North Coast Medical Inc., Morgan Hill, California, USA) with calibrated bending forces (Tamae et al., 2005). Rats were placed individually in an acrylic cap (12 cm in diameter, 7 cm in height, and weighing 256 g) with a wire mesh bottom. After the rats

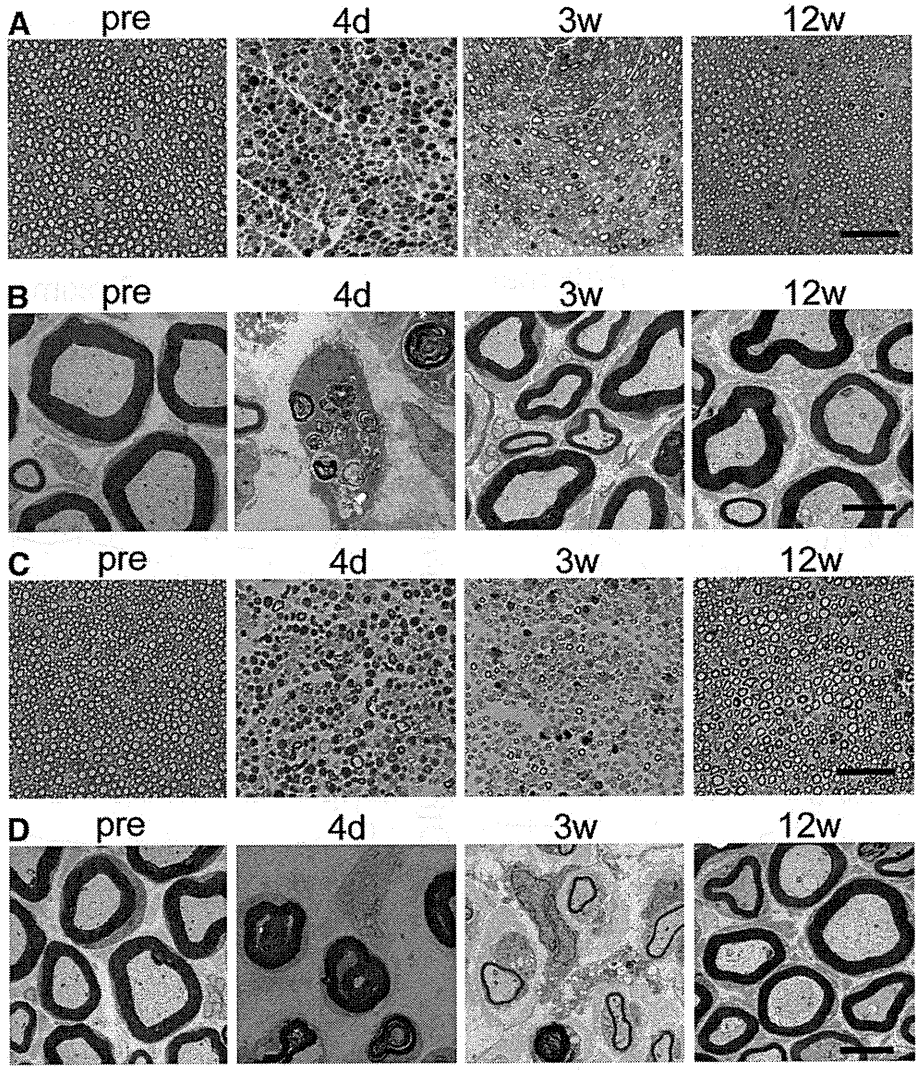

Fig. 3. Histological changes in the peripheral nerves at the lesion epicenter and at the distal site. Sections of 1 μm (A), stained with toluidine blue, and 80 nm (B), stained with uranyl acetate, were obtained from the lesion epicenter. Loss of axons and myelin debris arising from demyelination were observed 4 days after the injury (A). The phagocytosis of myelin debris by macrophages was observed (B). At 3 weeks after the injury, as the amount of myelin debris and number of macrophages decreased, myelinated axons became prominent. At 12 weeks after the injury, a similar number of myelinated axons to that in the pre-injury sciatic nerve was observed (A, B). Sections of 1 μm (C) stained with toluidine blue, and 80 nm (D) stained with uranyl acetate, were obtained from the site distal to the lesion epicenter. The series indicates that the axonal structures began to disintegrate within 4 days after the injury, then the axons began to regenerate by 3 weeks after the injury, and reached almost the pre-injury level of maturity by the end of the experimental period (C). Myelin debris was frequently detected 4 days after the injury. Macrophage recruitment, presumably for phagocytosis of the myelin debris, and very small axons within thin myelin sheaths were observed 3 weeks after the injury, followed by the formation of myelinated axons (D). (AX, axon; MS, myelin sheath; SC, Schwann cell; M, macrophage; scale bar, (A, C) 50 μm, (B, D) 5 μm).

had adapted to the testing environment for 60 min, the von Frey filaments were pressed perpendicularly against the plantar skin and held for 3–5 s with the filaments slightly buckled. Lifting of the paw was recorded as a positive response. The filaments were applied to the point of bending, six times each, to the plantar surface of the left and right hind paw, i.e., for a total of 12 times per rat, at intervals of 5 s; the next lightest filament was chosen for each subsequent measurement. The paw withdrawal threshold was taken as the lowest force that caused 100% withdrawals, and was considered the mechanical nociceptive threshold. The threshold ratio of the contralateral sham-operated side to that of the injured side was averaged.

Statistical analysis

All values were presented as the mean ± standard error of the mean (SEM). Statistical significance was determined as $P<0.05$ using Dunnett's multiple comparison. Pearson's correlation coefficients were calculated to determine the correlations between the histological/functional parameters and the diffusion imaging parameters. The SPSS statistical analysis software (version 16.0) was used for the analyses (SPSS Japan Inc., Tokyo, Japan).

Results

Diffusion tensor tractography and fractional anisotropy of injured peripheral nerves

We generated FA maps and delineated DTT images of the rat sciatic nerve for 12 weeks after contusive injury. On the FA maps (Fig. 1A), a sharp decrease in the intensity at the lesion epicenter was noted 3 h after the injury; thereafter, the intensity recovered gradually, reaching the pre-injury level by 4 weeks after the injury. At the distal site, the intensity was still preserved at both 3 h and 1 day; however, it was significantly decreased 4 days after the injury, and recovered gradually thereafter, reaching pre-injury levels by 4 weeks after the injury. Since tracking of the sciatic nerve depends on the selected FA threshold, at which the tracking is stopped, we also delineated DTT images of the sciatic nerves for 12 weeks after the injury using different FA thresholds: 0.25, 0.3, 0.4, 0.5, 0.6, 0.7, or 0.75 (Supplementary Figs. 1A–G). We found that the DTT images obtained using a FA threshold value of 0.4 (Fig. 1B) clearly showed the recovery process of the contused nerves. At 3 h after the injury, the fibers from the designated proximal site could not be tracked beyond the lesion epicenter, and fiber tracking could not proceed beyond the lesion epicenter until 1 day after the injury. On the other hand, a few fibers could be tracked distally by 4 days after the injury. The tractography revealed a return of the tracking parameters to the pre-injury levels, close those of the normal sciatic nerve, by 3 weeks after the injury.

Table 2
Correlations of the diffusion imaging parameters (Pearson's r) with the histological parameters

	Axon density	Axon diameter	Myelin density	Myelin thickness
FA	0.8618****	0.9166****	0.2387	−0.6941*
λ_1	0.9605****	0.9607****	0.4449	−0.5780

* $P<0.05$.
**** $P<0.001$.

To analyze the changes in the anisotropy of the injured sciatic nerves by DTI, we measured the FA values for 12 weeks after the injury. There were no significant changes in the FA value at the proximal site at any time point examined (Fig. 2A). In contrast, at the lesion epicenter, a sharp decrease in the FA value was observed 3 h after the injury, which then recovered gradually, reaching the pre-injury level by 3 weeks after the injury (Fig. 2B). In the images of the distal site, while no significant change in the FA value was observed at 3 h or 1 day, a decrease in the FA value was observed at 4 days, followed by gradual recovery thereafter, to the pre-injury level by 3 weeks after the injury (Fig. 2C).

We next analyzed the individual eigenvalues. The first eigenvalue (λ_1), which represents the diffusivity along the longitudinal axis of the nerve, was substantially higher than the second (λ_2) and third (λ_3) eigenvalues, which represent the diffusivity in directions perpendicular to the longitudinal axis. These radial diffusivities (λ_2 and λ_3) were much lower than the diffusivity value along the axis of the tract (λ_1). Thus, the present model showed that both λ_2 and λ_3 were more constant than λ_1 (Figs. 2D–F), and that the changes in the FA values after peripheral nerve injury depended mainly on λ_1, which represents the diffusivity along the longitudinal axis of the nerve.

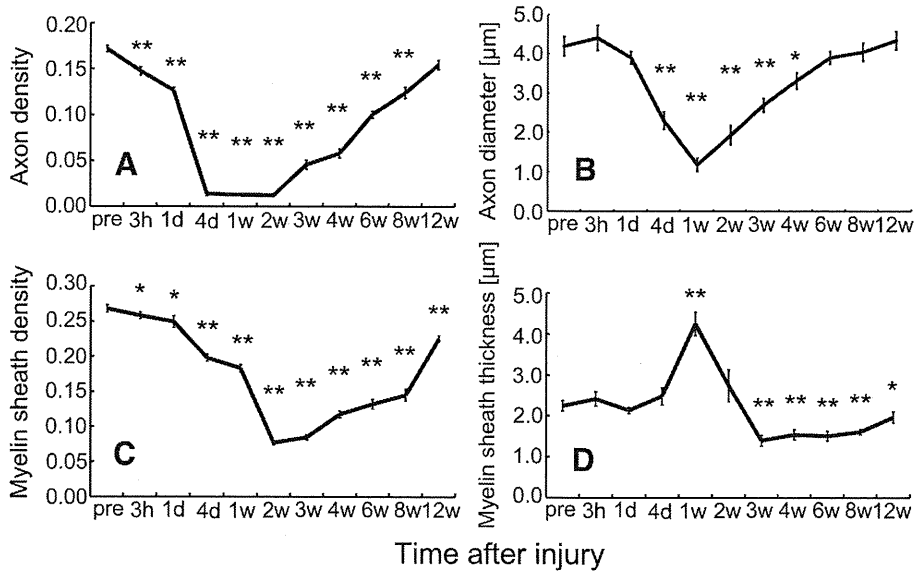

Fig. 4. Quantitative and temporal analysis of the axon density (myelinated axon area / total sectioned nerve area) (A), axon diameter (B), myelin sheath density (myelin sheath area / total sectioned nerve area) (C), and myelin sheath thickness (D) at the nerve site distal to the lesion epicenter ($n=10$ each). Statistical significance was determined to be $P<0.05$ using Dunnett's multiple comparison. Data represent the mean ± SEM. *$P<0.05$; **$P<0.01$.

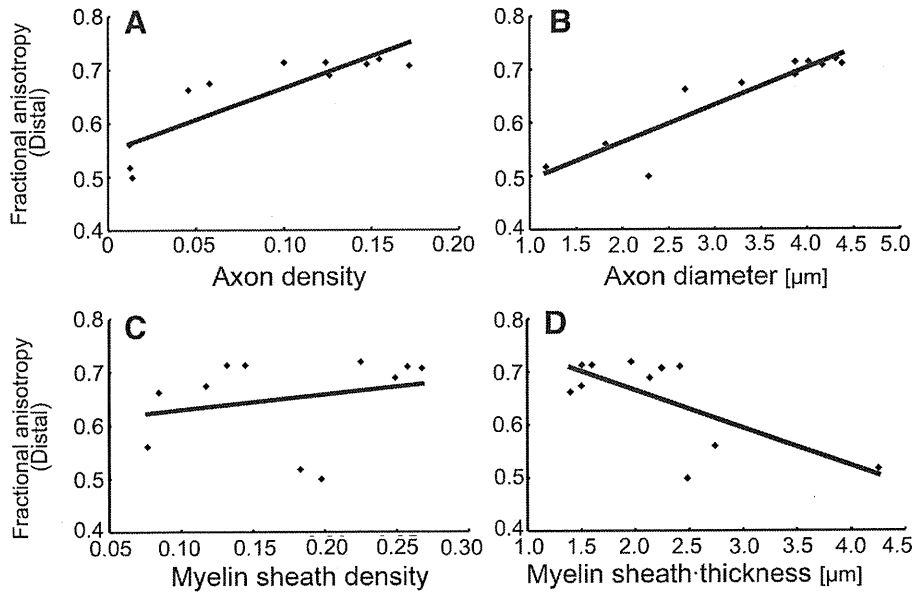

Fig. 5. Correlations between FA values and histological parameters. The FA values at the distal site were strongly correlated with each of the axonal parameters (A, Axon density, $r=0.8618$, $P=0.0006$; B, Axon diameter, $r=0.9166$, $P=0.0001$; C, Myelin sheath density, $r=0.2387$, $P=0.4796$; D, Myelin sheath thickness, $r=-0.6941$, $P=0.0178$).

Histological changes in the injured peripheral nerves

To examine the histological changes in the axons and myelin sheaths in detail, we performed toluidine blue and uranyl acetate staining of the nerves at the lesion epicenter and the distal site. At the lesion epicenter, axon loss and myelin debris arising from demyelination were observed 4 days after the injury (Fig. 3A). Consistent with these findings, EM examination revealed myelin debris being phagocytosed by macrophages (Fig. 3B). Subsequently, 3 weeks after the injury, as the amount of myelin debris and number of macrophages decreased, and myelinated axons began to appear prominently. At 12 weeks after the injury, myelinated axons similar in appearance and number to those in the pre-injury sciatic nerve were observed (Figs. 3A and B). At the distal site 4 days after the injury, more myelin debris and greater irregularity of the myelin sheaths were observed compared with the lesion epicenter (Figs. 3C and D), and fewer phagocytic macrophages were detected than at the lesion epicenter. A few regenerating axons, which appeared to be myelinated axons of smaller caliber with a thinner myelin sheath compared to normal axons, could be detected at 3 weeks, and these axons gradually reached the pre-injury level of maturity by 12 weeks after the injury (Fig. 3C). Three weeks after the injury, there was still a little myelin debris, which was being phagocytosed by macrophages, and a few small axons with thin myelin sheaths. These immature myelinated axons became progressively more mature and prominent with a thick myelin sheath, and the regenerated axons appeared similar to the axons observed pre-injury, by 12 weeks after the injury (Fig. 3D).

To analyze these changes quantitatively, we focused on the distal site, at which the Wallerian degeneration and regeneration could be clearly observed. We measured the number of axons, and the ratio of the myelinated axon area to the total sectioned nerve area as the axon density. The axon density decreased immediately after the nerve injury, reaching a minimum between 4 days and 2 weeks after the injury, and recovered gradually thereafter (Fig. 4A).

At this distal site, we also measured the ratio of the myelin sheath area to the total sectioned nerve area as the myelin sheath density. The myelin sheath density decreased gradually, reaching a minimum value 2 weeks after the injury, and began to recover thereafter (Fig. 4C). In addition, the axon diameter and myelin sheath thickness were measured in ultrathin (80 nm) sections under the electron microscope. No significant change in the axon diameter was noted until 1 day after the injury. Thereafter, with the swelling and degeneration of the myelin sheath, the axon diameter began to decrease, reaching a minimum at 1 week, and then recovered to the pre-injury level by 6 weeks after the injury (Fig. 4B), Furthermore, there was an obvious change in the pattern of axon diameter distribution pre and post injury (Supplementary Fig. 2). In contrast, the myelin sheath thickness increased to its maximum value at

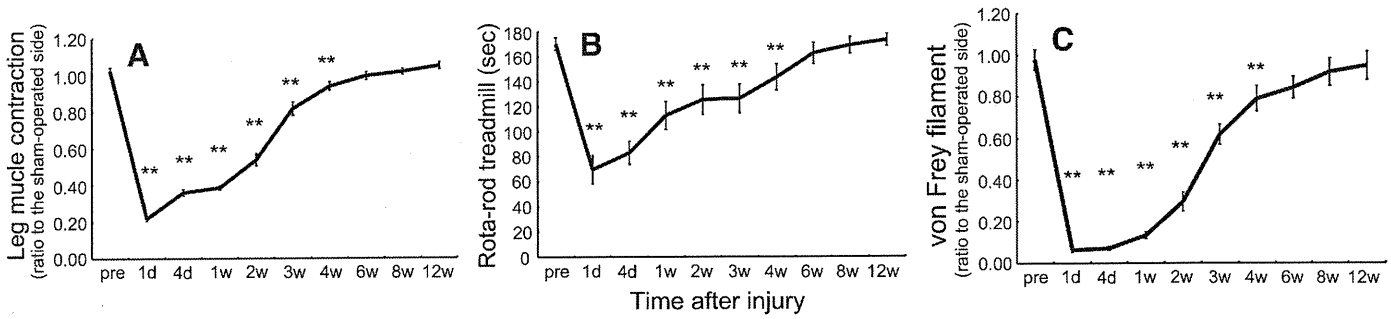

Fig. 6. Temporal analysis of the recovery of motor function in the lower extremities by the leg muscle contraction test (A), of motor coordination by the Rota-rod test (B), and of mechanical sensitivity by the von Frey filament test (C) for 12 weeks after contusion injury of the nerve. All three behavioral evaluations revealed functional recovery within 6 weeks of the nerve injury in this experimental model. Statistical significance was determined to be $P<0.05$ using Dunnett's multiple comparison. Data represent the mean ± SEM. *$P<0.05$; **$P<0.01$.

Table 3
Correlations of the diffusion imaging parameters (Pearson's *r*) with the functional parameters

	Leg muscle contraction	Rota-rod treadmill	von Frey filament
FA	0.9851****	0.9451****	0.9667****
λ_1	0.9591****	0.9695****	0.9355****

**** $P<0.001$.

1 week, due to swelling of the degenerated myelin sheath, and decreased gradually thereafter, accompanied by the disappearance of myelin debris. Regenerating axons with a thin myelin sheath began to appear by 2–3 weeks after the injury. A few more small, regenerating axons with a myelin sheath thinner than that observed pre-injury were detected at 3–8 weeks, and their number approached the pre-injury level by 12 weeks, accompanied by maturation of the myelin sheaths (Fig. 4D).

Almost all the histological axonal parameters were correlated with the FA and λ_1 values at the distal site. The FA value, a parameter used to construct the DTT, was most strongly correlated with the axon density and axon diameter ($P<0.001$) (Table 2 and Fig. 5).

Functional recovery after peripheral nerve injury

We next investigated whether the changes in FA values and histological parameters were associated with functional recovery, using three different behavioral tests. To evaluate the recovery of motor function, we measured the degree of leg muscle contraction, and assessed the forelimb-hindlimb motor coordination using the Rota-rod treadmill test. Both of these tests showed the full recovery of motor function by 6 weeks after the injury ($P<0.05$) (Figs. 6A and B). Sensory function was evaluated using the von Frey filament test. Marked impairment was observed 1 day after the injury, after which the values gradually improved, returning to pre-injury levels by 6 weeks ($P<0.05$) (Fig. 6C). Thus, all three behavioral evaluations revealed functional recovery within 6 weeks in this experimental model.

The FA and λ_1 values at the lesion epicenter showed strong correlations with each of the aforementioned functional parameters ($P<0.001$) (Table 3 and Fig. 7).

Discussion

Methodological considerations

Beaulieu et al. reported that Wallerian degeneration after peripheral nerve injury reduces the anisotropy of water diffusion (Beaulieu et al., 1996; Stanisz et al., 2001). Their findings indicated that DTT might be useful for depicting the changes in anisotropy after peripheral nerve injury, and thus has tremendous potential as a tool for diagnosing peripheral nerve injury. However, although several preliminary studies for the DTT of peripheral nerves have been performed (Hiltunen et al., 2005; Meek et al., 2006; Skorpil et al., 2004), none has fully explored the potential of the DTI technology, especially its ability to depict the degeneration and regeneration of peripheral nerves after injury.

To apply DTT as a novel clinical tool for evaluating peripheral nerve injury, it is first necessary to acquire accurate data for visualizing Wallerian degeneration and regeneration. In the present study, we used a highly reproducible model, in which the rat sciatic nerve was subjected to contusive injury using an aneurysm clip, with a constant holding force. The histological changes in our model were similar to those in previously reported models of axonotmesis (Bridge et al., 1994; Varejao et al., 2004), in which spontaneous regeneration at a distal nerve section and functional recovery were also observed. We used 7.0-Tesla MRI to obtain the images, employing a conventional spin-echo protocol rather than echo planar imaging, to minimize distortion of the images due to phase errors accumulation during the data acquisition. To reduce motion artifacts, the MR images of excised nerves were obtained. Since previous studies have demonstrated degradation of the diffusion anisotropy in excised models (Madi et al., 2005; Matsuzawa et al., 1995), we captured all the images immediately after dissection of the sciatic nerve.

Interpretation of the diffusion anisotropy

The FA value at the lesion epicenter decreased immediately after the injury. On the other hand, at the distal site, while no significant change in the FA value was observed at 3 h or 1 day after the injury, a significant decrease in the value was observed 4 days after the injury. These results were consistent with the histological findings, which showed that the axons and myelin were preserved in the nerve segment distal to the lesion epicenter up to 1 day after the injury, with disintegration of the axonal structures and demyelination (Wallerian degeneration), being observed 4 days after the injury. The perineurium, the sheath of connective tissue that surrounds each neural fascicle, was still preserved (Lundborg, 2004; Sunderland, 1991) and regulated the diffusivity. As a result, while the axon density decreased to nearly zero (Fig. 4A) in the preserved fascicles, a less than 30% drop in the FA value was observed at 4 days after the injury. Thereafter, the FA value recovered gradually, reaching its pre-injury level by 3 weeks after the injury, when a few regenerating axons could be detected; that is, the FA value at the distal site returned to its pre-injury level prior to the histological recovery. Furthermore, the FA values at the lesion epicenter during recovery showed extremely strong correlations with each of the functional parameters examined.

To clarify the relevance of the changes in the FA values after peripheral nerve injury, we examined the correlations between the FA values and the quantitative changes in axonal properties. The FA values of the peripheral nerves were more strongly correlated with the axonal density and diameter than with the myelin density and thickness. These findings support the theories that the axonal

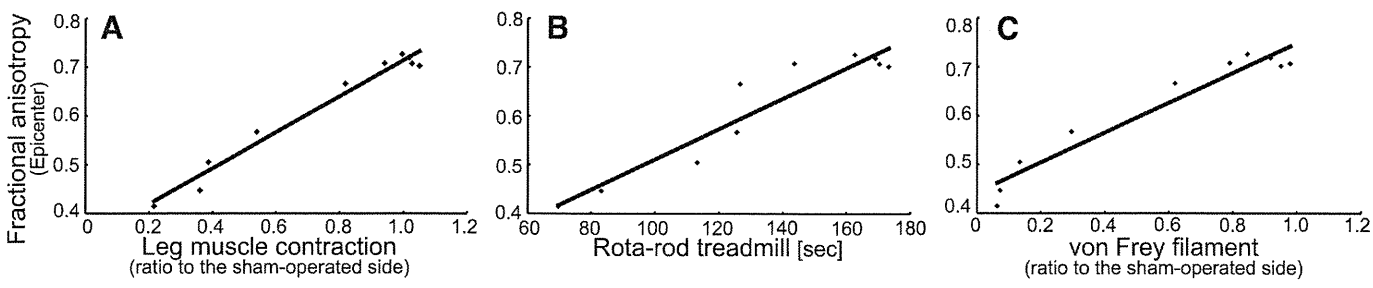

Fig. 7. Correlations between FA values and functional parameters. The FA values at the lesion epicenter were strongly correlated with each of the functional parameters (A, leg muscle contraction, $r=0.9851$, $P=0.000001$; B, Rota-rod treadmill, $r=0.9451$, $P=0.00004$; C, von Frey filament, $r=0.9667$, $P=0.000005$).

membranes play a major role in the anisotropic water diffusion in neural fibers (Beaulieu, 2002; Takahashi et al., 2002) and that myelination can modulate the degree of anisotropy (Gulani et al., 2001). The changes in the FA values after nerve injury mainly depended on λ_1, i.e., the axial diffusivity, consistent with the idea that water molecules preferentially diffuse along the longitudinal axis of axons, and degradation of the axonal cylinders would cause a loss of axial diffusivity. In addition, the absence of any significant change in the radial diffusivities (λ_2 and λ_3) might be explained by the present imaging conditions not being adequate to detect subtle changes of the radial diffusivities, which were significantly smaller than the axial diffusivity.

Potential clinical uses

Because it is difficult to distinguish peripheral nerves clearly from the surrounding tissues in conventional T1- and T2-weighted images, visualization of the Wallerian degeneration and regeneration of peripheral nerves after injury by MRI has been a challenge (Bendszus et al., 2002; Bendszus and Stoll, 2003; Bendszus et al., 2005; Filler et al., 1993; Howe et al., 1992; Kikuchi et al., 2003). In the present study, we were able to visualize these changes in peripheral nerves using DTI, and good correlations were found between the recovery as assessed by the changes in FA values and by histological and functional parameters. These findings support the applicability of DTI to the diagnosis of peripheral nerve injuries and monitoring of pathological conditions, to obtain information about the early phases of recovery in a clinical context.

We note that fiber tracking can sometimes terminate abruptly, because sharp bending or branching of the nerve can reduce the anisotropy below the tracking threshold (Hiltunen et al., 2005); therefore, the appropriate positioning and selection of a segment without branches will be critical, unless the spatial or angular resolution of the diffusion is greatly increased. In addition, although we have demonstrated the tracking and analysis of a straight sciatic nerve from the rat, which measures 1–1.5 mm in diameter and corresponds to the diameter of cutaneous nerves in humans, in voxels 0.31 mm in size, it is also important to keep in mind that the voxels forming the basis of the tracking are considerably larger than any individual axonal tract (Fujiyoshi et al., 2007).

We attempted to perform an in vivo study in a live model using smaller nerves to determine the feasibility of this method for clinical use (see Supplementary Materials), and we were able to demonstrate the recovery process of contused nerves in the same animal by tractography (Supplementary Fig. 3). Thus, DTT of the peripheral nerves could become an innovative tool for the evaluation of peripheral nerve injury, if applied correctly and with a clear understanding of its properties and limitations.

Acknowledgments

This work was supported by grants from the Leading Project for Realization of Regenerative Medicine from the Ministry of Education, Culture, Sports, Science and Technology (MEXT), Japan, from the Japan Science and Technology Corporation (JST), and from the General Insurance Association of Japan. This work was also supported by a Keio University grant-in-aid for encouragement of young medical scientists, by grants-in-aid for scientific research of MEXT, Japan, and by a grant-in-aid from the 21st Century COE Program of MEXT, Japan to Keio University. We thank Tokuko Harada and Hisako Takeuchi for tender animal care, Toshihiro Nagai for technical assistance with the electron microscope, and to all the other members of the spinal cord injury research team at Keio University School of Medicine for their enthusiastic discussions, encouragement, and invaluable comments on this study.

The authors declare no competing financial interests.

Appendix A. Supplementary data

Supplementary data associated with this article can be found, in the online version, at doi:10.1016/j.neuroimage.2008.09.022.

References

Basser, P.J., Mattiello, J., LeBihan, D., 1994. MR diffusion tensor spectroscopy and imaging. Biophys. J. 66, 259–267.
Beaulieu, C., 2002. The basis of anisotropic water diffusion in the nervous system – a technical review. NMR Biomed. 15, 435–455.
Beaulieu, C., Does, M.D., Snyder, R.E., Allen, P.S., 1996. Changes in water diffusion due to Wallerian degeneration in peripheral nerve. Magn. Reson. Med. 36, 627–631.
Bendszus, M., Stoll, G., 2003. Caught in the act: in vivo mapping of macrophage infiltration in nerve injury by magnetic resonance imaging. J. Neurosci. 23, 10892–10896.
Bendszus, M., Koltzenburg, M., Wessig, C., Solymosi, L., 2002. Sequential MR imaging of denervated muscle: experimental study. AJNR Am. J. Neuroradiol. 23, 1427–1431.
Bendszus, M., Wessig, C., Schutz, A., Horn, T., Kleinschnitz, C., Sommer, C., Misselwitz, B., Stoll, G., 2005. Assessment of nerve degeneration by gadofluorine M-enhanced magnetic resonance imaging. Ann. Neurol. 57, 388–395.
Bridge, P.M., Ball, D.J., Mackinnon, S.E., Nakao, Y., Brandt, K., Hunter, D.A., Hertl, C., 1994. Nerve crush injuries – a model for axonotmesis. Exp. Neurol. 127, 284–290.
Conturo, T.E., Lori, N.F., Cull, T.S., Akbudak, E., Snyder, A.Z., Shimony, J.S., McKinstry, R.C., Burton, H., Raichle, M.E., 1999. Tracking neuronal fiber pathways in the living human brain. Proc. Natl. Acad. Sci. U. S. A. 96, 10422–10427.
Filler, A.G., Howe, F.A., Hayes, C.E., Kliot, M., Winn, H.R., Bell, B.A., Griffiths, J.R., Tsuruda, J.S., 1993. Magnetic resonance neurography. Lancet 341, 659–661.
Filler, A.G., Maravilla, K.R., Tsuruda, J.S., 2004. MR neurography and muscle MR imaging for image diagnosis of disorders affecting the peripheral nerves and musculature. Neurol. Clin. 22, 643–682 vi-vii.
Fujiyoshi, K., Yamada, M., Nakamura, M., Yamane, J., Katoh, H., Kitamura, K., Kawai, K., Okada, S., Momoshima, S., Toyama, Y., Okano, H., 2007. In vivo tracing of neural tracts in the intact and injured spinal cord of marmosets by diffusion tensor tractography. J. Neurosci. 27, 11991–11998.
Gulani, V., Webb, A.G., Duncan, I.D., Lauterbur, P.C., 2001. Apparent diffusion tensor measurements in myelin-deficient rat spinal cords. Magn Reson Med 45, 191–195.
Hiltunen, J., Suortti, T., Arvela, S., Seppa, M., Joensuu, R., Hari, R., 2005. Diffusion tensor imaging and tractography of distal peripheral nerves at 3 T. Clin. Neurophysiol. 116, 2315–2323.
Howe, F.A., Filler, A.G., Bell, B.A., Griffiths, J.R., 1992. Magnetic resonance neurography. Magn. Reson. Med. 28, 328–338.
Kato, N., Nemoto, K., Nakanishi, K., Morishita, R., Kaneda, Y., Uenoyama, M., Ikeda, T., Fujikawa, K., 2005. Nonviral HVJ (hemagglutinating virus of Japan) liposome-mediated retrograde gene transfer of human hepatocyte growth factor into rat nervous system promotes functional and histological recovery of the crushed nerve. Neurosci. Res. 52, 299–310.
Kikuchi, Y., Nakamura, T., Takayama, S., Horiuchi, Y., Toyama, Y., 2003. MR imaging in the diagnosis of denervated and reinnervated skeletal muscles: experimental study in rats. Radiology 229, 861–867.
Lundborg, G., 2004. Nerve Injury and Repair, second ed. Elsevier, Philadelphia.
Mac Donald, C.L., Dikranian, K., Bayly, P., Holtzman, D., Brody, D., 2007a. Diffusion tensor imaging reliably detects experimental traumatic axonal injury and indicates approximate time of injury. J. Neurosci. 27, 11869–11876.
Mac Donald, C.L., Dikranian, K., Song, S.K., Bayly, P.V., Holtzman, D.M., Brody, D.L., 2007b. Detection of traumatic axonal injury with diffusion tensor imaging in a mouse model of traumatic brain injury. Exp. Neurol. 205, 116–131.
Madi, S., Hasan, K.M., Narayana, P.A., 2005. Diffusion tensor imaging of in vivo and excised rat spinal cord at 7 T with an icosahedral encoding scheme. Magn. Reson. Med. 53, 118–125.
Masutani, Y., Aoki, S., Abe, O., Hayashi, N., Otomo, K., 2003. MR diffusion tensor imaging: recent advance and new techniques for diffusion tensor visualization. Eur. J. Radiol. 46, 53–66.
Matsuzawa, H., Kwee, I.L., Nakada, T., 1995. Magnetic resonance axonography of the rat spinal cord: postmortem effects. J. Neurosurg. 83, 1023–1028.
Meek, M.F., Stenekes, M.W., Hoogduin, H.M., Nicolai, J.P., 2006. In vivo three-dimensional reconstruction of human median nerves by diffusion tensor imaging. Exp. Neurol. 198, 479–482.
Mori, S., Zhang, J., 2006. Principles of diffusion tensor imaging and its applications to basic neuroscience research. Neuron 51, 527–539.
Pierpaoli, C., Basser, P.J., 1996. Toward a quantitative assessment of diffusion anisotropy. Magn. Reson. Med. 36, 893–906.
Skorpil, M., Karlsson, M., Nordell, A., 2004. Peripheral nerve diffusion tensor imaging. Magn. Reson. Imaging 22, 743–745.
Song, S.K., Sun, S.W., Ju, W.K., Lin, S.J., Cross, A.H., Neufeld, A.H., 2003. Diffusion tensor imaging detects and differentiates axon and myelin degeneration in mouse optic nerve after retinal ischemia. Neuroimage 20, 1714–1722.
Stanisz, G.J., Midha, R., Munro, C.A., Henkelman, R.M., 2001. MR properties of rat sciatic nerve following trauma. Magn. Reson. Med. 45, 415–420.
Stejskal, E.O., Tanner, J.E., 1965. Spin diffusion measurements: spin echoes in the presence of a time dependent field gradient. J. Chem. Phys. 42, 288–292.
Sun, S.W., Liang, H.F., Cross, A.H., Song, S.K., 2008. Evolving Wallerian degeneration after transient retinal ischemia in mice characterized by diffusion tensor imaging. Neuroimage 40, 1–10.
Sunderland, S.S., 1991. Nerve Injuries and Their Repair: a Critical Appraisal. Churchill Livingstone, New York.
Takahashi, M., Hackney, D.B., Zhang, G., Wehrli, S.L., Wright, A.C., O'Brien, W.T., Uematsu, H., Wehrli, F.W., Selzer, M.E., 2002. Magnetic resonance microimaging of

intraaxonal water diffusion in live excised lamprey spinal cord. Proc. Natl. Acad. Sci. U. S. A. 99, 16192–16196.
Tamae, A., Nakatsuka, T., Koga, K., Kato, G., Furue, H., Katafuchi, T., Yoshimura, M., 2005. Direct inhibition of substantia gelatinosa neurones in the rat spinal cord by activation of dopamine D2-like receptors. J. Physiol. 568, 243–253.
Tuch, D.S., Wedeen, V.J., Dale, A.M., George, J.S., Belliveau, J.W., 2001. Conductivity tensor mapping of the human brain using diffusion tensor MRI. Proc. Natl. Acad. Sci. U. S. A. 98, 11697–11701.
Varejao, A.S., Cabrita, A.M., Meek, M.F., Bulas-Cruz, J., Melo-Pinto, P., Raimondo, S., Geuna, S., Giacobini-Robecchi, M.G., 2004. Functional and morphological assessment of a standardized rat sciatic nerve crush injury with a non-serrated clamp. J. Neurotrauma 21, 1652–1670.
Wessig, C., Jestaedt, L., Sereda, M.W., Bendszus, M., Stoll, G., 2008. Gadofluorine M-enhanced magnetic resonance nerve imaging: comparison between acute inflammatory and chronic degenerative demyelination in rats. Exp. Neurol. 210, 137–143.

Journal of Neuroscience Research 87:307–317 (2009)

Evaluation of Human Fetal Neural Stem/Progenitor Cells as a Source for Cell Replacement Therapy for Neurological Disorders: Properties and Tumorigenicity After Long-Term In Vitro Maintenance

Daisuke Ogawa,[1,2] Yohei Okada,[1,3] Masaya Nakamura,[4] Yonehiro Kanemura,[5] Hirotaka James Okano,[1] Yumi Matsuzaki,[1] Takuya Shimazaki,[1] Mamoru Ito,[6] Eiji Ikeda,[7] Takashi Tamiya,[2] Seigo Nagao,[2] and Hideyuki Okano[1]*

[1]Department of Physiology, School of Medicine, Keio University, Tokyo, Japan
[2]Department of Neurological Surgery, Faculty of Medicine, Kagawa University, Kagawa, Japan
[3]Department of Neurology, Graduate School of Medicine, Nagoya University, Nagoya, Japan
[4]Department of Orthopedic Surgery, School of Medicine, Keio University, Tokyo, Japan
[5]Institute for Clinical Research, Osaka National Hospital, National Hospital Organization, Osaka, Japan
[6]Central Institute for Experimental Animals, Tokyo, Japan
[7]Department of Pathology, School of Medicine, Keio University, Tokyo, Japan

It is expected that human neural stem/progenitor cells (hNS/PCs) will some day be used in cell replacement therapies. However, their availability is limited because of ethical issues, so they have to be expanded to obtain sufficient amounts for clinical application. Moreover, in-vitro-maintained hNS/PCs may have a potential for tumorigenicity that could be manifested after transplantation in vivo. In the present study, we demonstrate the in vitro and in vivo properties of long-term-expanded hNS/PCs, including a 6-month bioluminescence imaging (BLI) study of their in vivo tumorigenicity. hNS/PCs cultured for approximately 250 days in vitro (hNS/PCs-250) exhibited a higher growth rate and greater neurogenic potential than those cultured for approximately 500 days in vitro (hNS/PCs-500), which showed greater gliogenic potential. In vivo, both hNS/PCs-250 and -500 differentiated into neurons and astrocytes 4 weeks after being transplanted into the striatum of immunodeficient mice, and hNS/PCs-250 exhibited better survival than hNS/PCs-500 at this time point. We also found that the grafted hNS/PCs-250 survived stably and differentiated properly into neurons and astrocytes even 6 months after the surgery. Moreover, during the 6-month observation period by BLI, we did not detect any evidence of rapid tumorigenic growth of the grafted hNS/PCs, and neither PCNA/Ki67-positive proliferating cells nor significant malignant invasive features were detected histologically. These findings support the idea that hNS/PCs may represent a nontumorigenic, safe, and appropriate cell source for regenerative therapies for neurological disorders.

Key words: neural stem cell; in vivo optical imaging; long-term cultures; long-term engraftment; immunodeficient mouse

Recent progress in stem cell biology has greatly raised the expectation that cell replacement therapies may be developed for a variety of neurological disorders, such as spinal cord injury and neurodegenerative diseases, by using human fetal neural stem/progenitor cells (hNS/PCs) (Reynolds and Weiss, 1992; Svendsen et al., 1998; Carpenter et al., 1999; Uchida et al., 2000; Caldwell et al., 2001; Keyoung et al., 2001; Okano, 2002; Jeong et al., 2003; McBride et al., 2004; Cummings et al., 2005; Iwanami et al., 2005). However, the limited availability of human fetal tissues for ethical reasons makes it difficult to obtain large amounts of hNS/PCs. Therefore, for clinical applications, it is important to be able to expand hNS/PCs in vitro in a manner that maintains their multipotency and ability to self-renew.

Additional Supporting Information may be found in the online version of this article.

Contract grant sponsor: Leading Project for Realization of Regenerative Medicine from the Ministry of Education, Culture, Sports, Science and Technology (MEXT) of Japan; Contract grant sponsor: Japan Science and Technology Agency (SORST); Contract grant sponsor: Ministry of Health, Labor, and Welfare (to H.O.); Contract grant sponsor: Research Fellowships for Young Scientists from the Japan Society for the Promotion of Science (to Y.O.); Contract grant sponsor: Grant-in-Aid for 21st Century COE Program from the MEXT (to Keio University).

*Correspondence to: Hideyuki Okano, MD, PhD, Department of Physiology, Keio University School of Medicine, 35 Shinanomachi, Shinjuku-ku, Tokyo 160-8582, Japan. E-mail: hidokano@sc.itc.keio.ac.jp

Received 29 March 2008; Revised 12 June 2008; Accepted 13 June 2008

Published online 28 October 2008 in Wiley InterScience (www.interscience.wiley.com). DOI: 10.1002/jnr.21843

In addition, because of their low proliferation rate, it takes a long time for hNS/PCs to be expanded from a small number of cells to a sufficient population to use in cell replacement therapies. However, previous in vitro studies showed that subjecting hNS/PCs to multiple passages for up to 300 days in vitro (DIV) reduces their growth rate and alters their neurogenic potential (Caldwell et al., 2001; Kanemura et al., 2002; Piao et al., 2006; Wright et al., 2006; Anderson et al., 2007). Neither the proliferative and differentiation properties nor the in vivo dynamics have been reported for hNS/PCs cultured for longer than 300 DIV. Moreover, the long-term in vivo tumorigenicity of grafted hNS/PCs has never been described and is still uncertain.

Here we examined, both in vitro and in vivo, the differentiation and growth properties of hNS/PCs maintained for approximately 250 DIV (hNS/PCs-250) compared with hNS/PCs maintained for a longer period, approximately 500 DIV (hNS/PCs-500). Furthermore, we established a system for evaluating the in vivo tumorigenicity of hNS/PCs, by transplanting them into the striatum of immunodeficient mice and continuously monitoring the transplanted cells by bioluminescence imaging (BLI) in combination with conventional histology. With this system, we successfully monitored grafted cells for approximately 6 months, to evaluate the tumorigenicity of hNS/PCs as a source for cell replacement therapies.

MATERIALS AND METHODS

Cell Culture

Approval to use human fetal neural tissues and neurosphere cultures was obtained from the ethical committees of Keio University and Osaka National Hospital. Tissue procurement procedures were in accordance with the Declaration of Helsinki and in agreement with the ethical guidelines of the Japan Society of Obstetrics and Gynecology and with the ethical guidelines of the Network of European CNS Transplantation and Restoration (NECTAR). Forebrain tissues from a human fetus (8 weeks gestational age) were obtained from a legal abortion carried out at the Osaka National Hospital, with written informed consent obtained from the donor.

hNS/PCs were cultured using the neurosphere method (Reynolds and Weiss, 1992; Svendsen et al., 1998; Keyoung et al., 2001; Kanemura et al., 2002). The growth medium was a defined DMEM/F-12 (1:1)-based medium (Sigma, St. Louis, MO) supplemented with human recombinant (hr-) epidermal growth factor (20 ng/ml; PeproTech EC Inc., London, United Kingdom), hr-fibroblast growth factor 2 (20 ng/ml; PeproTech EC Inc.), hr-leukemia inhibitory factor (10 ng/ml; Chemicon, Temecula, CA), heparin (5 μg/ml; Sigma), B27 supplement (Invitrogen, Carlsbad, CA), and L-glutamine (200 mM; Invitrogen). Half of the culture medium was replaced with fresh growth medium every week. Neurospheres were passaged every 14 days by dissociating them into single cells using TrypLE select (Invitrogen). Viable cells (2×10^6 cells/15 ml) were seeded into 50% fresh growth medium plus 50% neurosphere-conditioned medium in uncoated T75 culture flasks and incubated at 37°C in 5% CO_2-95% air. hNS/PCs-250 represent neurospheres passaged 20–25 times; 244–314 DIV; mean 287.3 ± 24.2 DIV. hNS/PCs-500 represent neurospheres passaged 36–40 times; 476–526 DIV; mean 503.0 ± 18.8 DIV (mean ± SD).

To induce differentiation, the dissociated hNS/PCs were plated on poly-L-lysine (PLL)-coated coverslips and cultured in the DMEM/F-12/B27 without growth factors (Svendsen et al., 1998; Carpenter et al., 1999; Vescovi et al., 1999) for 7 days. On day 7, the cells were fixed in 4% paraformaldehyde (PFA) for 15 min and processed for immunocytochemical analysis.

Growth Assay

To measure the number of viable cells, the total ATP content was measured by ATP assay using the CellTiter-Glo Luminescent Cell Viability Assay (Promega, Madison, WI; Crouch et al., 1993; Petty et al., 1995). Single-cell suspensions were prepared from neurospheres by enzymatic dissociation with TrypLE select. The number of viable cells in the single-cell suspensions was determined by cell counting using trypan blue dye exclusion. To create a standard curve, 100-μl single-cell suspensions of known densities (1×10^5, 2×10^5, 4×10^5, and 8×10^5 cells/ml) were subjected to the ATP assay.

To assay the growth of hNS/PCs-250 and -500, single-cell suspensions from each neurosphere were plated in a 96-well plate (5×10^3 cells/100 μl). The cell number plated in each well on day 0 was equalized according to the ATP measurement, and the subsequent measurements were normalized to the value on day 0 (day 0 = 1, relative growth rate to day 0). Fresh medium (20 μl) was added every 4 days. The ATP assay was performed on days 0 (3 hr after plating), 2, 4, 7, and 11, by adding 100 μl of CellTiter-Glo Reagent to each well adjusted to 100 μl in advance. The luminescence signals were measured by a chemiluminescence detection system (Centro LB960; Berthold Technologies, Bad Wildbad, Germany).

Flow Cytometry

For cell-cycle analysis, the dissociated cells (1×10^6 cells) were incubated in 1 ml of hypotonic propidium iodide (PI) solution (1 mg/ml PI, 0.1% citric acid, 0.2% NP-40, 10 mg/ml RNaseA) (Deitch et al., 1982) for 30 min at 4°C, followed by a 15-min incubation at 37°C to digest the RNA. The fluorescent intensity of the PI was then measured by flow cytometry.

For the cell-surface marker analysis and viability assay, the dissociated cells were incubated in fresh medium at 37°C for 1 hr to recover the cell-surface antigens. The cells (1×10^7 cells) were suspended in 100 μl Hanks' balanced salt solution (HBSS) and incubated on ice for 30 min with allo phyco cyanin (APC)-conjugated anti-CD133 (Miltenyi Biotec, Tokyo, Japan) and phycoerythrin (PE)-conjugated anti-CD24 (BD Biosciences, Franklin Lakes, NJ), or fluorescvein isothiocyanate (FITC)-conjugated annexin V (BD Biosciences) to detect apoptosis. The cells were washed, resuspended in HBSS containing 1 μg/ml PI, and analyzed by FACS Caliber (BD Biosciences).

Virus Transduction and Bioluminescence Imaging

For the live monitoring of transplanted cells in vivo, we applied bioluminescent imaging (BLI), which has been described previously (Miyoshi et al., 1998; Okada et al., 2005). Human neurospheres and control U87MG cells were transduced by a lentivirus containing the click beetle red luciferase (CBR*luc*) coding sequence and Venus bicistronic reporter gene connected by an internal ribosomal entry site (IRES) (EF1α-CBRluc-IRES-Venus) (Supp. Info. Fig. 1A). The Venus-positive cells were then collected by a fluorescence-activated cell sorter (FACS) to establish cell lines that stably expressed Venus and CBR*luc*, as described previously (Masuda et al., 2007) (briefly summarized in Supp. Info. Fig. 1B). We confirmed that the photon counts from these CBR*luc*-labeled cells were directly proportional to the cell numbers plated in vitro (total cell numbers ranging from 10^2 to 10^6 cells/dish, Supp. Info. Fig. 1C,D). Moreover, the relative number of cells integrated into the host animals after transplantation could be estimated by measuring the photon counts from live animals after an intraperitoneal injection of D-luciferin. We also confirmed that the transduction with the lentivirus did not affect the proliferation or differentiation of hNS/PCs or the survival of the grafted animals (Supp. Info. Fig. 1E,F). A Xenogen-IVIS 100 cooled CCD optical macroscopic imaging system (Caliper Life Sciences, Hopkinton, MA) was used for BLI. All the images were analyzed with Igor (WaveMetrics, Lake Oswego, OR) and Living Image software (Caliper Life Sciences), and the optical signal intensity was expressed as photon counts, in units of photons per second. Each image was displayed as a pseudocolor photon count image superimposed on a gray-scale anatomic image. To quantify the measured luminescence, we defined a specific region of interest (ROI) that covered the area in and around the implanted cells. We used the same ROI for all the animals at all time points to ensure uniform data collection.

Transplantation

All the animal experiments were conducted according to the Guidelines for the Care and Use of Laboratory Animals of the Keio University School of Medicine. Mice were anesthetized and received implants of partially dissociated human neurospheres (2×10^6 cells in 4 μl of PBS) stereotactically into the right striatum (2 mm lateral and 1 mm anterior to bregma; depth 3 mm from dura). We used immunodeficient mice to avoid immunological rejection resulting from the xenograft. For short-term analyses of up to 4 weeks, we used *NOD/SCID/*γ_c^{null} (*NOG*) mice (Central Institute for Experimental Animals, Kanagawa, Japan), which are deficient for the common receptor gamma chain on the severe combined immunodeficiency (NOD/SCID) background (Ito et al., 2002) (n = 5 for hNS/PCs-250, n = 4 for hNS/PCs-500, n = 4 for U87MG). NOD/SCID mice (Charles River, Tokyo, Japan) were used for long-term observation of up to 6 months (n = 4 for hNS/PC-250, n = 4 for hNS/PCs-500, n = 4 for U87MG).

Animals were anesthetized and transcardially perfused with 4% PFA at 4 weeks (1 month), 12 weeks (3 months), and 24 weeks (6 months) after transplantation. The whole brain was removed and postfixed for 8 hr in 4% paraformaldehyde (PFA), soaked overnight in 15% followed by 30% sucrose, and embedded in OCT compound. Coronal sections 14 μm thick were made with a Cryostat (Leica, Wetzlar, Germany) and processed for immunohistochemical analysis.

Immunohistochemistry and Immunocytochemistry

For immunofluorescence analyses, cultured cells or tissue sections were incubated with the following primary antibodies at 4°C overnight: anti-human Nestin (1:30,000, rabbit polyclonal) (Nakamura et al., 2003), anti-TuJ-1 (1:500, mouse IgG2b monoclonal) (Sigma), antiglial fiibrillary acidic protein (GFAP) (1:3,000, rabbit polyclonal, Sigma), anti-green fluorescent protein (GFP; 1:25,000, mouse IgG2a, mFX72; a gift from Dr. S. Mitani), anti-Ki67 (1:500, Rb polyclonal IgG) (Novocastra Laboratories, Newcastle Upon Tyne, United Kingdom), antiproliferating cell nuclear antigen (PCNA) (1:1,000; Rb polyclonal IgG) (Oncogene, Boston MA), and anti-human nuclei (1:100, mouse monoclonal IgG1) (Chemicon). After three washes, the samples were incubated with Alexa 488-, 555-, or 647-conjugated secondary antibodies (Invitrogen) for 2 hr at room temperature. Images were obtained by microscopy (Apotome; Carl Zeiss) or confocal laser scanning microscopy (LSM510; Carl Zeiss).

The quantification of different phenotypes in vitro was accomplished by counting the immunolabeled cells on each coverslip. Five separate, randomly chosen fields on each coverslip were counted using a ×20 objective. The numbers of Nestin-, TuJ-1-, and GFAP-immunoreactive cells are presented as the percentage of total cells, which were stained by Hoechst 33258.

To quantify the Ki67-, PCNA-, and TUNEL-positive cells in tissue sections, the number of immunoreactive cells that were also positively stained by anti-human nuclei were counted in more than five randomly selected fields in each section. These data are presented as the percentage of total cells stained by human antinuclear antigen. Hematoxylin-eosin (HE) staining and HRP-DAB staining were carried out according to standard histological protocols.

Statistical Analysis

Statistical analyses were performed with Student's *t*-test and Dunn's test. Values are presented as the mean ± SEM. Significance was accepted at $P < 0.05$.

RESULTS

hNS/PCs Cultured for Long Periods Lost Their Proliferation Ability In Vitro

We first compared the properties of hNS/PCs-250 with those of hNS/PCs-500 in vitro, including the growth rate and differentiation potentials. By ATP assay (Kanemura et al., 2002), hNS/PCs-250 exhibited a significantly higher growth rate than did hNS/PCs-500 (Fig. 1A). Cell-cycle analysis by PI staining showed that the proportion of dividing cells in S/G2/M was 20.5% ± 1.2% for hNS/PCs-250, which was significantly higher than that for hNS/PCs-500 (12.7% ± 0.2%) (n = 3, $P < 0.01$; Fig. 1B). However, there was no

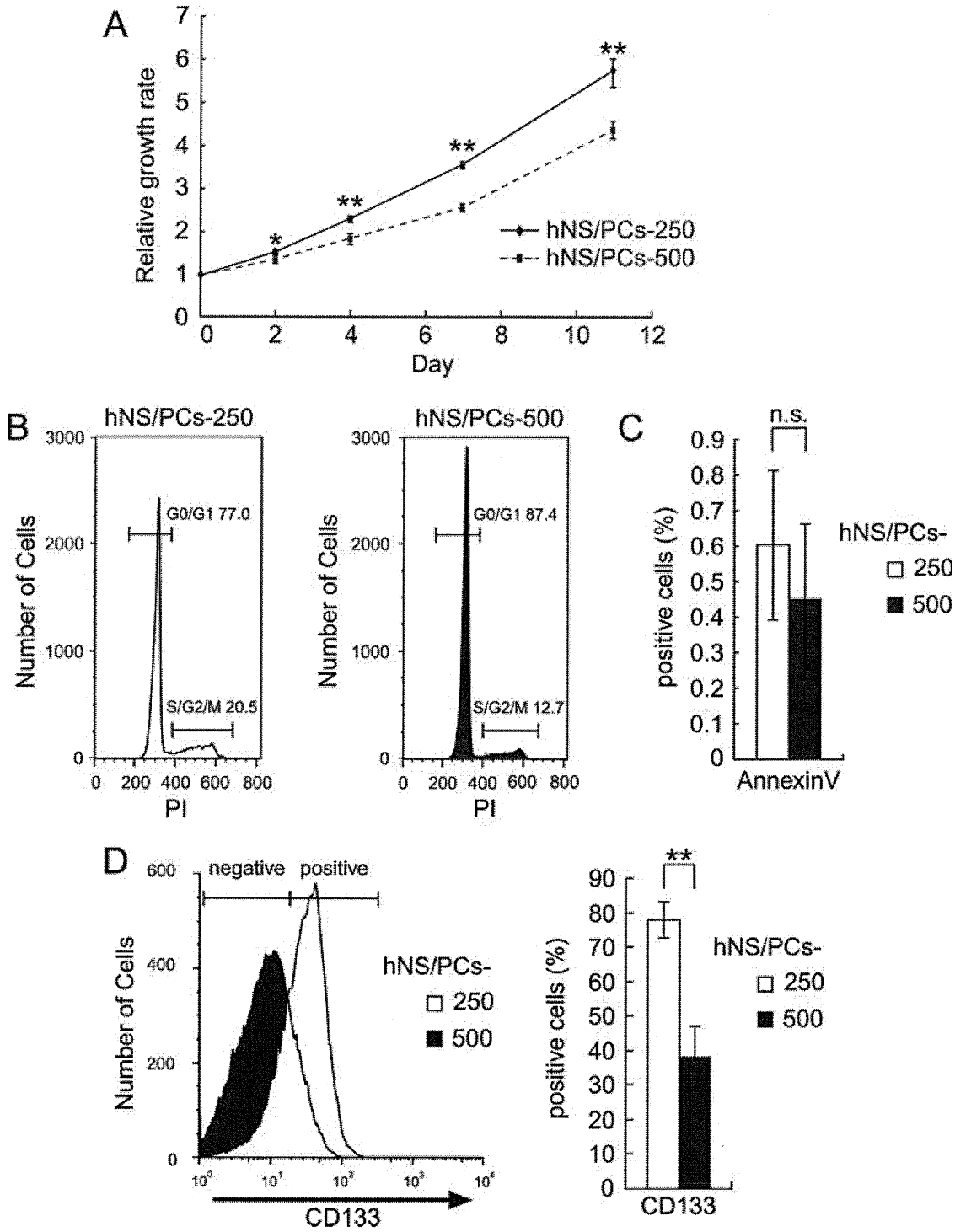

Fig. 1. Comparison of the in vitro properties of hNS/PCs-250 and -500. **A:** Growth rate of hNS/PCs-250 and -500 examined by ATP assay. hNS/PCs-250 exhibited a significantly higher growth rate than did hNS/PCs-500 during 11 days of culture. **B:** Cell-cycle analysis by PI staining. The proportion of dividing cells in S/G2/M was significantly higher in hNS/PCs-250 than in -500 ($P < 0.01$). **C:** Analysis of apoptotic cells by annexin V staining. No significant difference in the proportions of annexin V-positive cells was observed between hNS/PCs-250 and -500. n.s., Not significant ($P > 0.05$). **D:** Expression of CD133, a marker for undifferentiated hNS/PCs, in hNS/PCs-250 and -500 analyzed by flow cytometry. hNS/PCs-250 contained significantly more $CD133^+$ cells than did -500. All data are presented as the mean ± SEM (n = 3). $*P < 0.05$; $**P < 0.01$.

significant difference in the proportion of apoptotic cells stained with annexin V between hNS/PCs-250 and -500 (Fig. 1C). These results suggest that the difference in the in vitro growth rate between hNS/PCs-250 and -500 by ATP assay might be attributable to the presence of a differing proportion of proliferating cells, but not of apoptotic cells.

We speculated, based on these results, that there might be a difference in the proportion of undifferentiated hNS/PCs in the neurospheres of hNS/PCs-250 and -500. Therefore, we examined dissociated neurospheres for the expression of cell-type-specific surface markers by flow cytometry. The results indicated that the proportion of $CD133^+$ cells, which are known to represent an enriched population of neurosphere-initiating cells (Uchida et al., 2000; Barraud et al., 2007; Panchision et al., 2007), in hNS/PCs-250 was approximately twice that in hNS/PCs-500 (77.9% ± 5.2% and 38.2% ± 8.9% in hNS/PCs-250 and -500, respectively, $P < 0.01$; Fig. 1D), suggesting that the $CD133^+$ hNS/PCs in neurospheres may contribute to the higher growth rate seen in hNS/PCs-250 vs. hNS/PCs-500.

hNS/PCs-250 Generated Relatively More Neurons, Whereas hNS/PCs-500 Generated More Astrocytes

We next allowed hNS/PCs-250 and -500 to differentiate on PLL-coated coverglasses without growth factors for 7 days and examined their phenotypes by immunocytochemistry. There was no significant difference in the percentage of Nestin-positive cells between hNS/PCs-250 and -500 (Fig. 2A,B). However, whereas more than 50% of the hNS/PCs-250 differentiated into TuJ-1-positive neurons (54.3% ± 5.5% and 17.6% ± 3.0% in hNS/PCs-250 and -500, respectively, n = 3, $P < 0.01$), more than 70% of the hNS/PCs-500 differentiated into GFAP-positive astrocytes (23.6% ± 14.7% and 73.5% ± 6.6% in hNS/PCs-250 and -500, respectively, n = 3, $P < 0.05$). As previously reported, neither hNS/PCs-250 nor hNS/PCs-500 differentiated into CNPase-positive oligodendrocytes in vitro under the same conditions (Iwanami et al., 2005) (data not shown). Consistently with these findings, flow cytometric analyses showed that hNS/PCs-250 contained a greater proportion of $CD24^+$ cells, which are proposed to include the cells committed to neuronal lineages (Calaora et al., 1996; Shewan et al., 1996; Doetsch et al., 1999; Nieoullon et al., 2005; Panchision et al., 2007), than did hNS/PCs-500 (73.2% ± 5.4% and 56.1% ± 5.4% in hNS/PCs-250 and -500, respectively, n = 3, $P < 0.05$; Fig. 2C). Interestingly, most and some of the $CD24^+$ cells in the hNS/PCs-250 and -500 were also positive for CD133 (82.2% and 41.8%, respectively; Fig. 2D). Therefore, we also analyzed the $CD133^-$ populations and found that the proportion of $CD133^-$ cells that were $CD24^+$, possibly those representing neuronal progenitors and postmitotic neurons, tended to be higher in the hNS/PCs-250 than in the hNS/PCs-500, although the difference was not statistically significant (61.1% and 51.6% in hNS/PCs-250 and -500, respectively, $P = 0.06$; Fig. 2D). Taken together, these findings suggest that hNS/PCs-250 may contain more neurogenic progenitors than do the hNS/PCs-500, which contain more gliogenic progenitors.

hNS/PCs-250 Exhibited Better Survival After Transplantation Into the Striatum of NOG Mice Than Did hNS/PCs-500 by In Vivo Imaging

To assess the survival and differentiation potentials of hNS/PCs in vivo, we stereotactically transplanted hNS/PCs-250, hNS/PCs-500, or U87MG cells, a human glioblastoma cell line, into the right striatum of the intact mouse brain. To avoid immunological rejection of the grafted cells, we used NOG mice (Ito et al., 2002), which are deficient for the interleukin-2 receptor common γ chains under the background of severe combined immunodeficiency (NOD/SCID) mice (Shultz et al., 1995).

After transplantation, we observed the survival and growth of the grafted hNS/PCs and U87MG cells for up to 4 weeks (n = 4 each). For the live monitoring of transplanted cells in vivo, we labeled the hNS/PCs and U87MG with a lentivirus containing the coding sequence for CBR*luc* and a Venus reporter gene (EF1α-CBR*luc*-IRES-Venus) (Supp. Info. Fig. 1A) and applied BLI (Okada et al., 2005). The BLI results revealed that the surviving grafted hNS/PCs-250 and -500 decreased sharply, to approximately 20–40% of their original levels 1 week after the transplantation and were maintained thereafter. Four weeks after the transplantation, hNS/PCs-250 showed significantly better survival than did hNS/PCs-500 (12.7% ± 2.4% and 3.8% ± 1.0% of the initial photon counts in hNS/PCs-250 and -500, respectively, n = 4, $P < 0.01$; Fig. 3A,B). In contrast, the U87MG glioblastoma cells showed logarithmic growth during the 4-week observation period.

Immunohistochemical analyses revealed that both hNS/PCs-250 and hNS/PCs-500 had differentiated into TuJ1-positive neurons and GFAP-positive astrocytes 4 weeks after the transplantation (Fig. 4A). Nestin-positive neural progenitors were also observed in both the hNS/PCs-250 and the hNS/PCs-500 grafts. hNS/PCs-250 contained significantly more Ki67- and PCNA-positive cells than did hNS/PCs-500 (Ki67: 5.1% ± 0.8% and 3.1% ± 0.3%, $P < 0.05$; PCNA: 5.8% ± 0.2% and 4.4% ± 0.3%, in hNS/PCs-250 and -500, respectively, n = 3, $P < 0.01$; Fig. 4B,C). The percentage of TUNEL-positive apoptotic cells was not significantly different between hNS/PCs-250 and hNS/PCs-500 (0.26% ± 0.05% and 0.37% ± 0.14%, respectively, n = 3; Fig. 4D,E).

Grafted Neurospheres Survived and Differentiated Into Neurons and Astrocytes In Vivo but Did Not Show Tumorigenicity Even 6 Months After Transplantation

Finally, we evaluated the long-term survival of hNS/PCs and investigated their safety as a cell source